A Structure-Based 3D-QSAR Study of Anthrapyrazole Analogues of the Anticancer Agents Losoxantrone and Piroxantrone

Hong Liang,[†] Xing Wu,[†] Lynn J. Guziec,[‡] Frank S. Guziec, Jr.,[‡] Kimberly K. Larson,[‡] Jennifer Lang,[‡] Jack C. Yalowich,[§] and Brian B. Hasinoff*,[†]

Faculty of Pharmacy, University of Manitoba, Winnipeg, Manitoba R3T 2N2, Canada, Department of Chemistry, Southwestern University, Georgetown, Texas 78628, and Department of Pharmacology, University of Pittsburgh School of Medicine, Pittsburgh, Pennsylvania 15261

Received February 20, 2006

A series of 13 anthrapyrazole compounds that are analogues of piroxantrone and losoxantrone were synthesized, and their cell growth inhibitory effects, DNA binding, topoisomerase IIα mediated (EC 5.99.1.3) cleavage of DNA, and inhibition of DNA topoisomerase IIα decatenation catalytic activities were determined. Cell growth inhibitory activity was well-correlated with DNA binding, suggesting that these compounds may act by targeting DNA. However, cell growth inhibition was not well-correlated with the inhibition of topoisomerase IIα catalytic activity, suggesting that these anthrapyrazoles did not act solely by inhibiting the catalytic activity of topoisomerase II. Most of the analogues were able to induce DNA cleavage, and thus, it was concluded that they acted, at least in part, as topoisomerase II poisons. Structure-based three-dimensional quantitative structure−activity analyses (3D-QSAR) were carried out on the aligned structures of the anthrapyrazoles docked into DNA using comparative molecular field analysis (CoMFA) and comparative molecular similarity index (CoMSIA) analyses in order to determine the structural features responsible for their activity. Both CoMFA and CoMSIA yielded statistically significant models upon partial least-squares analyses. The 3D-QSAR analyses showed that hydrogen-bond donor interactions and electrostatic interactions with the protonated amino side chains of the anthrapyrazoles led to high cell growth inhibitory activity.

1. INTRODUCTION

Piroxantrone (DuP 942, CI-942, oxantrazole, or pirozantrone) and losoxantrone (DuP 941, CI 941, or biantrazole) are anthrapyrazole antitumor agents that were developed as noncardiotoxic alternatives to the quinone-containing anthracyclines doxorubicin and daunorubicin.[1−3] The clinical use of doxorubicin is usually limited by the development of a cumulative dose-dependent and potentially fatal cardiotoxicity, which is probably due to oxidative stress on the relatively unprotected cardiac muscle. These planar anthrapyrazole compounds can intercalate into DNA[4,5] and cause DNA strand breaks.[6] Both piroxantrone and losoxantrone likely exert their antitumor effects by acting as DNA topoisomerase II poisons.[7,8] We previously compared the chronic toxicity of piroxantrone, losoxantrone, and doxorubicin in a rat model.[9] A structure−activity study has shown that cell growth inhibitory activity was maximized by basic side chains at N-2 and C-5, two to three carbon spacers between proximal and distal nitrogens of the side chain, and A-ring hydroxylation.[5] More recently, aza-bioisosteres of the anthrapyrazoles have been developed and are now in clinical trials.[10,11] We have prepared an extended series of anthrapyrazoles and have carried out quantitative structure−activity relationship (QSAR) correlation and structure-based 3D-QSAR studies involving measurements of inhibition of topoisomerase IIα (EC 5.99.1.3), topoisomerase IIα mediated DNA cleavage, and DNA binding and docking of the analogues into DNA to determine the factors that affect the growth inhibitory effects of these compounds. Some of the analogues were designed with an alkylating group on the anthrapyrazole side chain in order to increase cytotoxicity by potentially covalently binding to DNA upon intercalation.

2. MATERIALS AND METHODS

2.1. Materials. pBR322 plasmid DNA was obtained from MBI Fermentas (Burlington, Canada) and the kinetoplast plasmid DNA (kDNA) from TopoGEN (Columbus, OH). HindIII was from Invitrogen (Burlington, Canada). Unless otherwise indicated, other chemicals were from Sigma (Oakville, Canada). The 3-(4,5-dimethylthiazol-2-yl)-5-(3-carboxymethoxyphenyl)-2-(4-sulfophenyl)-2H-tetrazolium (MTS) CellTiter 96 AQueous One Solution Cell Proliferation Assay kit was obtained from Promega (San Luis Obispo, CA). Losoxantrone and piroxantrone were obtained from the National Cancer Institute (Bethesda, MD). The linear least-squares analysis was done with SigmaStat (Systat, Point Richmond, CA).

2.2. Synthesis of the Anthrapyrazoles. The synthesis of AP-3, AP-7, AP-10, and AP-12 have been described.[5,12] The chloroanthrapyrazole derivatives AP-3 and AP-7 were prepared from commercially available 1,4- and 1,5-dichloroanthroquinone by reaction with 2-[(hydrazinoethyl)amino]-ethanol in refluxing acetonitrile.[13] AP-12 was prepared by reaction of 1,4-dichloroanthroquinone with 2-hydrazino-

* Corresponding author tel.: 204 474-8325; fax: 204 474-7617; e-mail: B_Hasinoff@UManitoba.ca.
[†] University of Manitoba.
[‡] Southwestern University.
[§] University of Pittsburgh School of Medicine

10.1021/ci060056y CCC: $33.50
Published on Web 05/18/2006

ethanol at 110 °C. The N-methylated derivatives AP-1 and AP-9 were prepared by reaction of the corresponding unmethylated compounds (AP-3 and AP-7) with formaldehyde in formic acid at 110 °C. The N,N′-disubstituted anthrapyrazoles AP-10, AP-11, AP-13, and AP-14 were prepared from the corresponding chloroanthrapyrazoles by reaction with excess *N*,*N*-dimethylethylenediamine at reflux. Chlorinated derivatives AP-2, AP-4, AP-6, and AP-8 were prepared from the corresponding hydroxy compounds by reaction with excess thionyl chloride at room temperature. Anthrapyrazole hydrochlorides and dihydrochlorides were prepared by the addition of excess methanolic hydrogen chloride followed by crystallization of the resulting solids from methanol/ether. All structures were confirmed by ^{1}H and ^{13}C nuclear magnetic resonance spectroscopy.

2.3. Cell Culture and Growth Inhibition Assays. Human leukemia K562 cells, obtained from the American Type Culture Collection and K/VP.5 cells (a 26-fold etoposide-resistant K562-derived subline with decreased levels of topoisomerase IIα mRNA and protein)[14−17] were maintained as suspension cultures in Dulbecco's Modified Eagle Medium (Invitrogen, Burlington, Canada) containing 10% fetal calf serum and 2 mM L-glutamine. The spectrophotometric 96-well plate cell growth inhibition MTS assay, which measures the ability of the cells to enzymatically reduce MTS after drug treatment, has been described.[18,19] The drugs were dissolved in dimethylsulfoxide (DMSO). The final concentration of DMSO did not exceed 0.5% (v/v) and was an amount that had no detectable effect on cell growth. The cells were incubated with the drugs for the times indicated and then assayed with MTS. The 50% cell growth inhibitory concentration (IC_{50}) values for growth inhibition in both assays were measured by fitting the absorbance−drug concentration data to a four-parameter logistic equation as described.[18]

2.4. Topoisomerase IIα kDNA Decatenation Inhibition Assay. A spectrofluorometric decatenation assay was used to determine the inhibition of topoisomerase IIα by the anthrapyrazoles.[20−22] kDNA consists of highly catenated networks of circular DNA. Topoisomerase IIα decatenates kDNA in an ATP-dependent reaction to yield individual minicircles of DNA. The 20 μL reaction mixture contained 0.5 mM ATP, 50 mM Tris-HCl (pH 8.0), 120 mM KCl, 10 mM $MgCl_2$, 30 μg/mL bovine serum albumin, 50 ng of kDNA, the test compound (0.5 μL in dimethylsulfoxide), and 20 ng of topoisomerase IIα protein (the amount that gave approximately 80% decatenation). Using a high copy yeast expression vector, full-length human topoisomerase IIα was expressed, extracted, and purified as described previously.[22] The final dimethylsulfoxide concentration of 2.5% (v/v) was shown in controls not to affect the activity of topoisomerase IIα. The assay incubation was carried out at 37 °C for 20 min and was terminated by the addition of 12 μL of 250 mM Na_2EDTA. Samples were centrifuged at 8000*g* at 25 °C for 15 min, and 20 μL of the supernatant were added to 180 μL of 600-fold diluted PicoGreen dye (Molecular Probes, Eugene, OR) in a 96-well plate. The fluorescence, which was proportional to the amount of kDNA, was measured in a Fluostar Galaxy (BMG, Durham, NC) fluorescence plate reader using an excitation wavelength of 485 nm and an emission wavelength of 520 nm.

2.5. pBR322 DNA Relaxation and Cleavage Assays. Topoisomerase II cleaved DNA complexes produced by anticancer drugs may be trapped by rapidly denaturing the complexed enzyme with sodium dodecyl sulfate (SDS).[23] The anthrapyrazole-induced cleavage of double-stranded closed circular pBR322 DNA to form linear DNA was followed by separating the SDS-treated reaction products using ethidium bromide gel electrophoresis as described.[23] The 20 μL cleavage assay reaction mixture contained a 100 μM sample of the drug, 150 ng of topoisomerase IIα protein, 80 ng of pBR322 plasmid DNA (MBI Fermentas, Burlington, Canada), and 0.5 mM ATP in an assay buffer [10 mM Tris-HCl, 50 mM KCl, 50 mM NaCl, 0.1 mM EDTA, 5 mM $MgCl_2$, 2.5% (v/v) glycerol, pH 8.0, and the drug (0.5 μL in dimethylsulfoxide)]. The order of addition was assay buffer, DNA, drug, and then topoisomerase IIα. The reaction mixture was incubated at 37 °C for 10 min and quenched with 1% (v/v) SDS/25 mM Na_2EDTA. The reaction mixture was treated with 0.25 mg/mL proteinase K (Sigma) at 55 °C for 30 min to digest the protein. The linear pBR322 DNA cleaved by topoisomerase IIα was separated by electrophoresis (2 h at 8 V/cm) on a TAE {Tris base (4 mM)/glacial acetic acid [0.11% (v/v)]/Na_2EDTA (2 mM) buffer/ethidium bromide (0.5 μg/mL)/agarose gel (1.2%, wt/v)}. Ethidium bromide was used in the gel and running buffer in order that the inhibition of relaxation activity could be measured along with the formation of cleaved linear DNA. The DNA in the gel was imaged by its fluorescence on an Alpha Innotech (San Leandro, CA) Fluorochem 8900 imaging system equipped with a 365 nm UV illuminator and a CCD camera.

2.6. Thermal Denaturation of DNA Assay. Compounds that intercalate into DNA stabilize the DNA double helix and increase the temperature at which the DNA is denatured.[11,24,25] The effect of 2 μM of the compounds on the DNA thermal melt temperature (T_m) of sonicated calf thymus DNA (5 μg/mL) was measured in 10 mM Tris-HCl buffer (pH 7.5) in a Cary 1 (Varian, Mississauga, Canada) double-beam spectrophotometer by measuring the absorbance increase at 260 nm upon the application of a temperature ramp of 1 °C/min. The maximum of the first derivative of the absorbance−temperature curve was used to obtain the T_m. Doxorubicin (2 μM), which is a strong DNA intercalator, was used as a positive control.[24] Under limiting conditions, the value of ΔT_m is directly proportional to the logarithm of the equilibrium constant for ligand binding to DNA,[25] and thus, the value of ΔT_m was used directly in the free-energy correlation analyses.

2.7. Docking of the Anthrapyrazoles into an X-ray Structure of DNA. All molecular modeling was done using SYBYL 7.0[26] on a Hewlett-Packard XW4100 PC workstation with a Redhat Enterprise 3 Linux operating system. All molecules except the DNA were built using SYBYL. The mono- or diprotonated anthrapyrazoles with one or two amino side chains, respectively, were docked into the doxorubicin binding site of a six-base-pair (bp) X-ray crystal structure of two molecules of doxorubicin bound to double-stranded DNA, d(TGGCCA)/doxorubicin (http://www.rcsb.org/pdb/; PDB ID: 1DA9),[27] using the genetic algorithm docking program GOLD version 2.2[28] and using the default GOLD parameters.[29] GOLDScore was used as the fitness function with flipping options of amide bonds, planar and pyramidal nitrogens, and internal hydrogen bonds being allowed. No early termination was allowed.

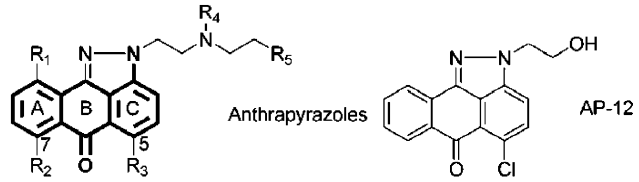

Compound	R_1	R_2	R_3	R_4	R_5
AP-1	H	H	Cl	CH_3	OH
AP-2	H	H	Cl	CH_3	Cl
AP-3	H	H	Cl	H	OH
AP-4	H	H	Cl	H	Cl
AP-6	H	Cl	H	CH_3	Cl
AP-7	H	Cl	H	H	OH
AP-8	H	Cl	H	H	Cl
AP-9	H	Cl	H	CH_3	OH
AP-10	H	H	$NH(CH_2)_2N(CH_3)_2$	H	OH
AP-11	H	H	$NH(CH_2)_2N(CH_3)_2$	CH_3	OH
AP-13	H	$NH(CH_2)_2N(CH_3)_2$	H	H	OH
AP-14	H	$NH(CH_2)_2N(CH_3)_2$	H	CH_3	OH
Losoxantrone	H	OH	$NH(CH_2)_3NH(CH_2)_2OH$	H	OH
Piroxantrone	OH	OH	$NH(CH_2)_3NH_2$	H	OH

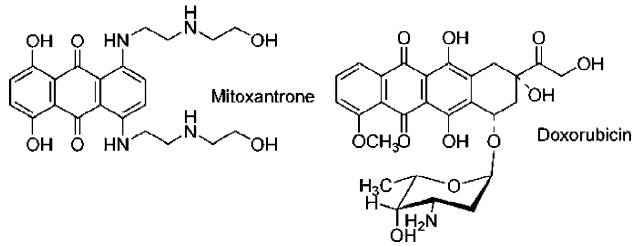

Figure 1. Structures of the anthrapyrazoles, mitoxantrone, and doxorubicin. The core structure used for alignment of the anthrapyrazoles for the 3D-QSAR CoMFA and CoMSIA is shown in bold.

The 1DA9 X-ray structure shows that the first and second base pairs buckle out to accommodate bound doxorubicin.[27,30] Thus, the 1DA9 X-ray structure of the doxorubicin−DNA complex was used for the docking experiments, rather than constructing DNA in SYBYL, because it was reasoned that this DNA structure would be a more realistic model for the binding of anthrapyrazoles because of their structural similarity to doxorubicin (Figure 1). The protonated anthrapyrazoles were first geometry optimized with the Tripos force field[31] using a conjugate gradient with a convergence criterion of 0.01 kcal/mol and Gasteiger−Huckel charges and a distance-dependent dielectric constant. The SYBYL CONFORT module was then used to find the lowest-energy conformation. The DNA structure was prepared by removing one of the bound doxorubicin molecules and removing all of the water molecules to avoid potential interference with the docking. Hydrogens were added to the DNA, and the SYBYL Biopolymer module was used to add Kollman-All charges[32] to the DNA. Using bound doxorubicin as the reference ligand, the binding site was defined as being within 5 Å of the reference ligand. The anthrapyrazoles, losoxantrone, piroxantrone, and mitoxantrone were all docked into the DNA structure to obtain the top 10 scoring GOLDScore structures for each molecule. Each of these structures was then rescored using a local optimization (simplexing) to obtain the final GOLDScore and their individual component energy terms. Rescoring did not affect the initial relative scoring order. The GOLD fitness function (GOLDScore) is the sum of its four components: DNA−ligand hydrogen-bond energy (external H bond); DNA−ligand van der Waals (vdw) energy (external vdw); ligand internal vdw energy (internal vdw); and ligand torsional strain energy (internal torsion). And these were output for QSAR correlation analysis. The ligand intramolecular hydrogen-bond energy (internal H bond) term was zero for each docked ligand as there were no internal H bonds found in the docked structures. For the QSAR correlation analysis, the sum of the internal torsion and internal vdw terms was combined into the single internal energy term *S*(int) as these two terms were highly cross-correlated ($p = 2 \times 10^{-6}$). As a test of the docking procedure, doxorubicin was docked back into the DNA structure with a heavy-atom root-mean-squared distance of 1.3 Å compared to the X-ray structure.[27] Values of 2.0 Å or less in the extensive GOLD test set are considered to be good.[29]

2.8. Structure-based 3D-QSAR Analyses. Comparative molecular field analysis (CoMFA) and comparative molecular similarity index analysis (CoMSIA) require that the 3D structures of the molecules be aligned to a core conformational template that is their presumed active form.[33−35] The molecular conformations which were used for alignment were the conformers that had the best GOLDScore value after docking by GOLD. All of the molecules were then aligned to the template molecule AP-10, the most potent compound (shown in Figure 1 with the template atoms joined by heavy lines), by using the Align Database option in SYBYL. CoMFA and CoMSIA were also carried out on aligned structures in the lowest-energy conformations obtained with the SYBYL CONFORT module. For the CoMFA calculation, steric and electrostatic field energies were calculated using an sp^3 carbon with a van der Waals radius of 1.52 Å as the steric probe and a +1 charge as an electrostatic probe. Steric and electrostatic interactions were calculated using the Tripos force field with a distance-dependent dielectric constant at all lattice points of a regular spaced (2 Å) grid. The energy cutoff was 30 kcal/mol. The alignment and lattice box used for the CoMFA calculation were also used to calculate similarity index fields for the CoMSIA. Steric, electrostatic, hydrophobic, and hydrogen-bond donor and acceptor fields were evaluated in CoMSIA. Similarity indices were computed using a probe atom with a +1 charge, radius of 1 Å, hydrophobicity of +1, hydrogen-bond donating of +1, hydrogen-bond acceptor of +1, and an attenuation factor α of 0.3 for the Gaussian-type distance.

A partial least-squares (PLS) statistical approach, which is an extension of multiple regression analysis in which the original variables are replaced by a set of their linear combinations, was used to obtain the 3D-QSAR results. All models were investigated using the leave-one-out (LOO) method, which is a cross-validated partial least-squares method. The CoMFA and CoMSIA descriptors were used as independent variables, and pIC_{50} or ΔT_m were used as dependent variables to derive 3D-QSAR models. The q^2 (cross-validated correlation coefficient r^2) and the optimum number of components (*N*) were obtained by the LOO method. The final model (non-cross-validated conventional analysis) was developed and yielded the non-cross-validated correlation coefficient r^2 with the optimum number of components. Because it has been shown that losoxantrone was most closely related to the anthracenedione mitoxantrone and other topoisomerase II poisons in the NCI COMPARE analysis,[7] and because mitoxantrone has a core structure and side chains the same as or similar to those of the other

Table 1. DNA ΔT_m, Cytotoxicity, and Topoisomerase II Inhibitory Effects of the Anthrapyrazoles

		MTS cell growth inhibition			topo II inhibition
agent	ΔT_m (°C)	K562 IC_{50} (μM)	K/VP.5 IC_{50} (μM)	resistance factor[a]	IC_{50} (μM)
AP-1	7.0	4.9	6.2	1.3	2.9
AP-2	6.0	4.4	6.0	1.4	0.25
AP-3	9.1	1.8	2.5	1.4	13
AP-4	5.2	11	12	1.1	12
AP-6	6.3	6.2	6.2	1.0	0.87
AP-7	7.0	3.3	4.3	1.3	18
AP-8	8.0	6.3	8.6	1.4	14
AP-9	6.1	5.7	6.4	1.1	7.2
AP-10	25.0	0.11	0.26	2.4	23
AP-11	24.0	0.26	0.86	3.3	16
AP-12	0	11.9	21	1.7	9.2
AP-13	4.1	1.7	3.1	1.8	11
AP-14	17.0	0.30	0.60	2.0	19
losoxantrone	18.1	0.12	0.22	1.8	7.3
piroxantrone	19.0	4.0	6.7	1.7	4.6
mitoxantrone	18.4	0.42	1.68	4.0	5.3
doxorubicin	13.2	0.08	0.41	5.1	ND

[a] The resistance factor was calculated from the ratio of the IC_{50} value for the K/VP.5 cell line divided by that for the K562 cell line. ND is not determined.

anthrapyrazoles, it was included in the analysis of the other 15 anthrapyrazoles studied.

3. RESULTS

3.1. Effect of the Anthrapyrazoles on the Thermal Denaturation of DNA. Doxorubicin (2 μM), which is a well-known DNA intercalating drug, was used as a control and was observed to increase the ΔT_m of sonicated DNA by 13.2 °C from 71.0 °C. Of the anthrapyrazoles studied (Table 1), AP-10 had the largest effect on ΔT_m and, thus, was bound the strongest to DNA. By contrast, AP-12, which has no amino side chains (Figure 1), did not increase ΔT_m, which indicates that the amino side chains were important for DNA binding. It can be seen from the data in Figure 1 and Table 1 that, when a chlorine was substituted for an hydroxyl group on the pyrazole side chains in the pairs AP-1/AP-2, AP-3/AP-4, AP-9/AP-6, and AP-7/AP-8, the ΔT_m was either decreased or unaffected, and thus, it can be concluded that the hydroxyl group did not make a large contribution to the binding to DNA. For the AP-13/AP-14 pair, in which a hydrogen was substituted by a methyl group, the ΔT_m was increased, but for the AP-3/AP-1, AP-4/AP-2, AP-8/AP-6, AP-7/AP-9, and AP-10/AP-11 pairs for this substitution, the ΔT_m values were essentially unchanged. It can also be seen from the AP-10/AP-13 and AP-11/AP-14 pairs that moving the amino side chain from the 5- to the 7-ring position decreased ΔT_m, which suggests that having the two amino side chains on the same side of the anthrapyrazole, as in losoxantrone, piroxantrone, mitoxantrone, and favors binding to DNA.

3.2. Effect of the Anthrapyrazoles on Cell Growth Inhibition. As shown in Table 1, all of the anthrapyrazoles inhibited the growth of K562 and K/VP.5 cells. AP-10 was the most potent of the compounds, and AP-12, which has no amino side chains, was the least potent, indicating the importance of the amino side chains. It can be seen from the data in Table 1 that, when a chlorine was substituted for a hydroxyl group on the pyrazole side chains in the pairs

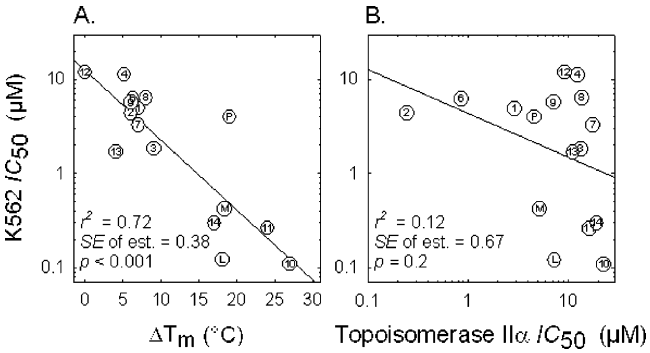

Figure 2. QSAR correlations of growth inhibition of K562 cells by the anthrapyrazoles and mitoxantrone. (A) The IC_{50} for growth inhibition of K562 cells by the anthrapyrazoles and mitoxantrone was highly significantly correlated ($p = 3 \times 10^{-5}$) with the strength of DNA binding as measured by their ability to increase the thermal melt temperature of DNA (ΔT_m). (B) The IC_{50} for growth inhibition of K562 cells by the anthrapyrazoles and mitoxantrone was not significantly correlated ($p = 0.2$) with the inhibition of the catalytic decatenation activity of topoisomerase IIα. The anthrapyrazoles are identified by the numbers inside the symbols, and losoxantrone, piroxantrone, and mitoxantrone are identified as L, P, and M, respectively.

AP-1/AP-2, AP-3/AP-4, AP-9/AP-6, and AP-7/AP-8, the growth inhibitory activity was either decreased or unaffected. Thus, it can be concluded that the design goal of increasing cytotoxicity by having an alkylating group on the anthrapyrazole side chain was not achieved. The effect of converting the secondary amine group on the pyrazole side chain into a tertiary methylamine was mixed. For the AP-13/AP-14 pair, in which a hydrogen was substituted by a methyl group, the growth inhibitory effect was increased, but for the AP-3/AP-1, AP-4/AP-2, AP-8/AP-6, AP-7/AP-9, and AP-10/AP-11 pairs for this same substitution, growth inhibitory effects were either unchanged or slightly reduced. It can also be seen from the AP-10/AP-13 and AP-11/AP-14 pairs that moving the amino side chain from the 5- to the 7-ring position decreased or did not affect growth inhibitory effects, respectively.

3.3. The Anthrapyrazoles Inhibit the Decatenation Activity of Topoisomerase IIα. As shown in Table 1, all of the anthrapyrazoles inhibited the decatenation activity of human topoisomerase IIα. This assay is a measure of the ability of these compounds to inhibit the catalytic activity only and was not a measure of whether these compounds acted as topoisomerase II poisons as do losoxantrone and piroxantrone[7,8] and some widely used anticancer drugs.[36,37] It can be seen from the data in Table 1 that AP-10, which was the most potent in terms of growth inhibition, was the weakest inhibitor of topoisomerase IIα.

3.4. QSAR Correlation Analyses of DNA Binding Affinity and Topoisomerase IIα Inhibition. As shown in Figure 2A, the logarithm of the K562 IC_{50} data was well-correlated with ΔT_m ($r^2 = 0.72$ and $p = 3 \times 10^{-5}$), which indicates that a high binding affinity for DNA results in a high potency. This result suggests that these compounds target DNA or interfere with some enzyme that processes DNA. The logarithm of the K562 IC_{50} data was, however, poorly correlated with the IC_{50} for the catalytic inhibition of topoisomerase IIα ($r^2 = 0.12$ and $p = 0.2$; Figure 2B). The lack of correlation with topoisomerase IIα IC_{50} does not mean that these compounds did not act on topoisomerase

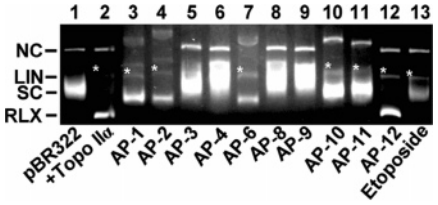

Figure 3. Effect of anthrapyrazoles on the topoisomerase IIα-mediated cleavage of supercoiled pBR322 DNA. This fluorescent image of the ethidium bromide-stained gel shows that topoisomerase IIα relaxed supercoiled pBR322 plasmid DNA (SC) to relaxed DNA (RLX). As shown in lane 2, topoisomerase IIα completely relaxed pBR322 DNA (lane 1, no enzyme). Topoisomerase IIα was present in the reaction mixture for all other lanes. As shown in lane 13, etoposide treatment produced linear DNA (LIN) and inhibited the relaxation of supercoiled pBR322 DNA. A small amount of nicked circular (NC) is normally present in the pBR322 DNA. Bands identified as linear DNA are marked above and to their left with an "*". AP-1, AP-2, AP-6, AP-10, AP-11, and AP-12 are identified as having produced linear DNA above control levels (lane 2). The binding of some of the fluorescent anthrapyrazoles (AP-3, AP-4, AP-8, and AP-9) to DNA obscured the band where the linear DNA would be expected to be found and also caused a mobility shift due to their binding. Topo IIα is topoisomerase IIα.

II as topoisomerase II poisons but only that they did not act solely through their inhibition of the catalytic activity of topoisomerase IIα.

3.5. Effect of Anthrapyrazoles on the Stabilization of the Covalent Topoisomerase IIα−DNA Cleavable Complex. Several widely used anticancer agents, including doxorubicin and the other anthracyclines, mitoxantrone, and etoposide,[36,37] as well as losoxantrone and piroxantrone,[7,8] are thought to be cytotoxic by virtue of their ability to stabilize a covalent topoisomerase II−DNA intermediate (the cleavable complex) and act as what are called topoisomerase II poisons. Topoisomerase II alters DNA topology by catalyzing the passing of an intact DNA double helix through a transient double-stranded break made in a second helix and is critical for relieving torsional stress that occurs during replication and transcription and for daughter-strand separation during mitosis.[36,37] Thus, DNA cleavage assay experiments[23] as we previously described[38] were carried out using 100 μM etoposide as a control to see whether 100 μM of the test compounds stabilized the cleavable complex. As shown in Figure 3, the addition of etoposide (lane 13) to the reaction mixture containing topoisomerase IIα and supercoiled pBR322 DNA induced the formation of linear pBR322 DNA and inhibited the relaxation of supercoiled pBR322 DNA. Linear DNA was identified by comparison with linear pBR322 DNA produced by action of the restriction enzyme HindIII acting on a single site on pBR322 DNA. The anthrapyrazoles were mixed in their ability to induce linear DNA formation. The interpretation of the results was problematic for some of the anthrapyrazoles, both because binding of the anthrapyrazoles to the DNA retarded the migration of the linear DNA band and also because of interference from the fluorescence of bound anthrapyrazole. Identification of the linear DNA bands in the former cases was aided by the identification of the shift of the nicked circular DNA. The latter effect could be largely, but not completely, ameliorated by destaining the gel overnight and restaining with ethidium bromide. For the anthrapyrazoles that could be evaluated, these experiments showed that AP-1, AP-2, AP-6, AP-10, AP-11, and AP-12 were able to induce the formation of linear DNA (marked on the gel image of Figure 3 with an "*"), indicating that these anthrapyrazoles, at least, were able to stabilize the covalent topoisomerase II−DNA intermediate. It is interesting that AP-12, which does not detectably intercalate into DNA (Table 1), produced the largest amount of linear DNA. It is likely that the anthrapyrazoles that strongly bind DNA inhibit the formation of linear DNA because of intercalation at higher concentrations as has been shown for doxorubicin.[39]

3.6. The Effects of the Anthrapyrazoles on the Growth of a K562 Cell Line Compared to the K/VP.5 Cell Line with a Decreased Level of Topoisomerase IIα. One method by which cancer cells increase their resistance to topoisomerase II poisons is by lowering their level or activity of topoisomerase II.[15,36] With less topoisomerase II in the cell, cells produce fewer DNA strand breaks and topoisomerase II poisons are less lethal to cells. These cell lines provide a convenient way to test whether a drug that inhibits topoisomerase II acts as a topoisomerase II poison.[22] Conversely, a lack of change in sensitivity of a putative topoisomerase II poison to a cell line with a lowered topoisomerase II level can be taken to indicate that poisoning of topoisomerase II was not an important mechanism for this particular agent. We previously showed that the K/VP.5 cell line with acquired resistance to etoposide contained one-fifth the topoisomerase IIα content of the parental K562 cells.[14−17] The IC_{50} values for growth inhibition of K562 and K/VP.5 cells, as measured with the MTS assay, after a 72 h continuous treatment with a range of anthrapyrazole concentrations are compared in Table 1. While almost all of the anthrapyrazoles except AP-2 were somewhat cross-resistant, none were as cross-resistant as mitoxantrone or doxorubicin (4- to 5-fold). Interestingly, the anthrapyrazoles AP-10 and AP-11 that were the most potent at inhibiting cell growth were also the most cross-resistant. Thus, from these results and the results of the cleavage assay (Figure 2), it can be concluded that most of the anthrapyrazoles inhibit cell growth, at least in part, by acting as topoisomerase II poisons.

3.7. Docking of the Anthrapyrazoles into DNA. The structure of AP-10, the most potent anthrapyrazole, docked into DNA is shown in Figure 4A. AP-10 shows both stacking interactions and H-bond interactions through both amino side chains with the DNA base pairs between which it intercalates. Additionally, the side-chain hydroxyl group forms a H bond with the oxygen of a DNA sugar residue. The conformations of all of the aligned anthrapyrazoles and mitoxantrone docked into DNA have been superimposed in Figure 4B. Most of the anthrapyrazoles docked into the DNA with a similar configuration, both with respect to the pyrazole rings and the amino side chains. However, some of the docked anthrapyrazoles were slightly rotated about the central DNA axis.

Linear regression (Figure 5A,B) was carried out on the logarithm of the K562 IC_{50} values versus the GOLD fitness function and each of its four component terms: (DNA−ligand hydrogen-bond energy (external H bond); DNA−ligand van der Waals (vdw) energy (external vdw); ligand internal vdw energy (internal vdw); and ligand torsional strain energy (internal torsion). A regression analysis of the ΔT_m data was also carried out (Figure 5C,D). Because ΔT_m and the logarithm of the K562 IC_{50} values were highly correlated ($p = 4 \times 10^{-5}$), the conclusions reached from the K562 IC_{50}

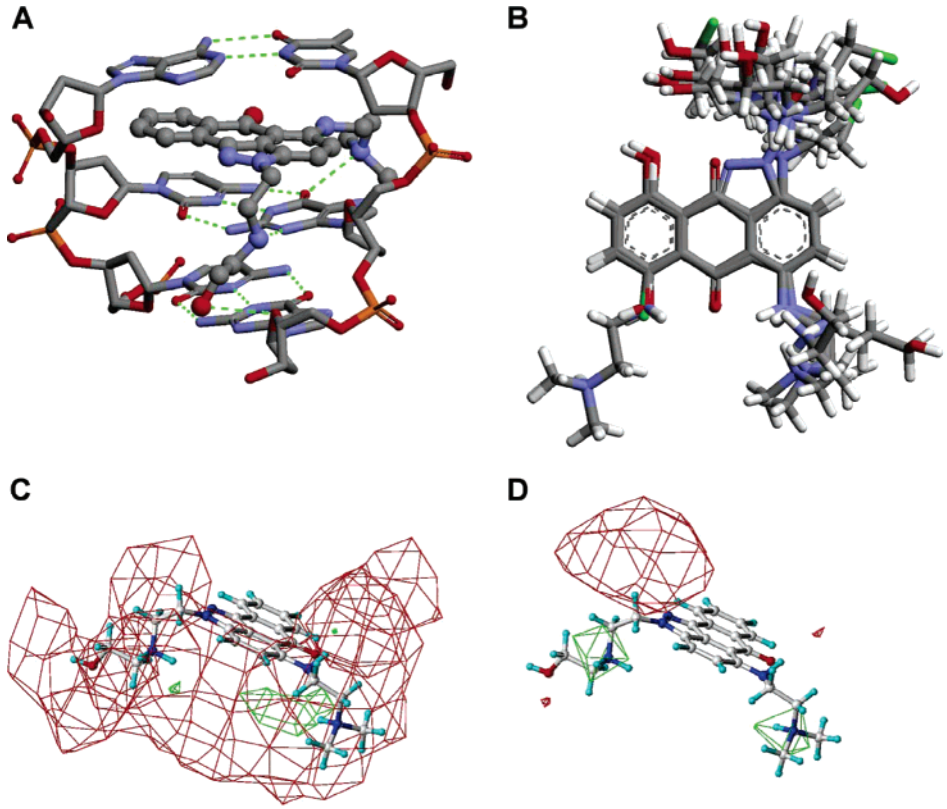

Figure 4. Docking of the protonated anthrapyrazoles into DNA, their aligned docked structures, and CoMSIA contour plots. (A) The highest-scoring structure of the most potent anthrapyrazole AP-10 (ball-and-stick structure) is shown docked into DNA (stick structure). The complex forms both base-stacking and H-bonding interactions (green dotted lines). The side chains of AP-10 formed three hydrogen bonds (one from the terminal OH and two others from the secondary and tertiary nitrogens) with DNA. The hydroxyl side chain of AP-10 was positioned in the minor groove, and the dimethyl amino side chain was in the major groove. The H atoms are not shown for clarity. The DNA structure is 1DA9 from the Protein Data Bank and is a doxorubicin/DNA X-ray structure in which two doxorubicin molecules are bound to a six-bp piece of DNA. Only the first three base pairs of the DNA are shown in the figure for clarity. One doxorubicin was removed, and AP-10 was docked into its place with the genetic algorithm docking program GOLD. (B) The structures of all the anthrapyrazoles and mitoxantrone that were docked into DNA and aligned to the core structure as shown in Figure 1 (bold bonds) are shown superimposed. (C) CoMSIA stddev*coeff contour hydrogen-bond donor plots for the K562 growth inhibition data are shown for AP-10, the most potent anthrapyrazole. The green contours indicate regions where hydrogen-bond donors increase activity, and the red contours indicate regions where hydrogen-bond donors decrease activity. The green contours were located near the nitrogens of the side chains, indicating the importance of these groups. (D) CoMSIA stddev*coeff contour electrostatic plots for the K562 growth inhibition data are shown for AP-10, the most potent anthrapyrazole. The green contours indicate regions where electrostatic interactions increase activity, and the red contours indicate regions where electrostatic interactions decrease activity. The green contours were located near the protonated nitrogens of the side chains, indicating the importance of protonated nitrogens in the activity of the anthrapyrazoles.

analysis likewise apply to the ΔT_m data shown in Figure 5C. While the overall GOLD fitness function was itself not well-correlated ($p = 0.2$), two of its component terms (external van der Waals and *S*(int), the sum of the two internal energy terms) were (Figure 5A). As shown in Figure 5A, an increase in the contribution to the external van der Waals energy term to the GOLD score was well-correlated ($p = 2 \times 10^{-4}$) with increasing growth inhibitory potency. Likewise, an increase in the external van der Waals energy term also corresponded to an increased binding affinity to DNA as shown in Figure 5C. For the ΔT_m data, this is a reasonable result as increased van der Waals interactions with DNA, in particular, would be expected to lead to increased binding affinity and increased growth inhibitory effects. Figure 5B, however, shows that an increase in the internal energy of the anthrapyrazoles decreases cell growth inhibitory properties (and also in weaker binding to DNA as shown in Figure 5D). The internal energy term reflects the internal torsional and van der Waals increases in energy because of conformational changes that the anthrapyrazoles must make to be able to dock into DNA. A conformational analysis of druglike molecules bound to proteins has shown that ligands often do not bind in their lowest-energy conformation.[40] However, for a series of structurally similar anthrapyrazoles, as were studied here, it is reasonable that an increase in the internal energy is negatively correlated with both ΔT_m and growth inhibitory effects.

3.8. Structure-based 3D-QSAR. The results of the CoMFA and CoMSIA on the K562 growth inhibitory IC_{50} and ΔT_m data of Table 1 are summarized in Table 2. The IC_{50} values for K562 cell growth inhibition and for inhibition of the activity of topoisomerase IIα each varied by approximately 100-fold. However, these IC_{50} values for both cell growth inhibition and inhibition of the enzyme were all measured by one person using a standard protocol, which increased the relative accuracy of the assay. In the case of the enzyme assay, a single preparation of the enzyme was used, which would also increase the relative accuracy of the assay. From our experience with these assays, it is estimated that we can replicate IC_{50} values to within 0.2 log units. As can be seen from Table 2, the standard error of the estimates (S. E. E.) of about 0.3 log units for the CoMFA and CoMSIA

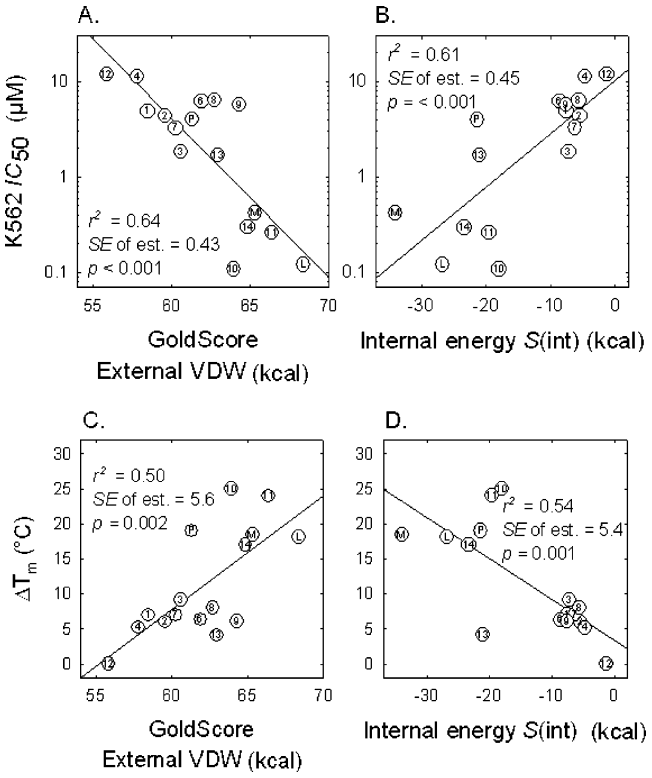

Figure 5. QSAR correlations of IC_{50} values for growth inhibition of K562 cells by the anthrapyrazoles and mitoxantrone with energy terms obtained by docking the anthrapyrazoles into a DNA X-ray structure. (A) The IC_{50} for growth inhibition of K562 cells by the anthrapyrazoles and mitoxantrone was highly correlated ($p = 2 \times 10^{-4}$) with the GOLDScore external van der Waals energy term in the GOLDScore fitness function, indicating that increased van der Waals interactions with DNA increase the potency of these compounds. (B) The IC_{50} for growth inhibition of K562 cells by the anthrapyrazoles and mitoxantrone was highly correlated ($p = 4 \times 10^{-4}$) with the GOLDScore internal energy term in the GOLDScore fitness function, indicating that increased internal energy (sum of internal torsion and internal van der Waals energies) of the docked compound interactions with DNA decreases the potency of these compounds. (C) The ΔT_m for the anthrapyrazoles and mitoxantrone were highly correlated ($p = 0.002$) with the GOLDScore external van der Waals energy term in the GOLDScore fitness function, indicating that increased van der Waals interactions with DNA increase the DNA binding of these compounds. (D) The ΔT_m for the anthrapyrazoles and mitoxantrone was highly correlated ($p = 0.001$) with the GOLDScore internal energy term in the GOLDScore fitness function, indicating that increased internal energy (sum of internal torsion and internal van der Waals energies) of the docked compound interactions with DNA decreases the DNA binding of these compounds. The anthrapyrazoles are identified by the numbers inside the symbols, and losoxantrone, piroxantrone, and mitoxantrone are identified as L, P, and M, respectively. In GOLD, a positive increase in an energy term corresponds to increased growth inhibitory activity or binding.

fits are similar to the estimated error in the measurements. The errors in the determination of ΔT_m are likely better than 0.5 °C. No compounds were excluded as outliers in the CoMFA or CoMSIA. Because of the relatively small numbers of compounds in the data set (16), all structures were used in the analyses rather than dividing them into training and validation sets. For these variables, the optimum number of components was one. The predicted and experimental values for the K562 IC_{50} and ΔT_m data are plotted in Figure 6A and B, respectively. The CoMFA and CoMSIA of the K562 IC_{50} data gave fairly high q^2 values (0.757 and 0.705, respectively), which indicates that the model and the

Table 2. PLS Statistics and Field Contributions of CoMFA and CoMSIA Models for the Prediction of pIC_{50} for K562 Cell Growth Inhibition and for ΔT_m for Binding of Anthrapyrazoles to DNA[a]

PLS Statistics						
	K562 pIC_{50}		ΔT_m (°C)		topo II pIC_{50}	
parameter	CoMFA	CoMSIA	CoMFA	CoMSIA	CoMFA	CoMSIA
q^2	0.757	0.705	0.593	0.570	0.305	0.147
N	1	1	1	1	3	1
S. E. P.	0.355	0.391	0.384	0.394	0.491	0.503
r^2	0.870	0.842	0.785	0.776	0.845	0.527
S. E. E.	0.260	0.286	0.279	0.285	0.232	0.357
F	93	75	51	48	21.7	15.6
Field Contributions						
steric	0.428	0.111	0.386	0.103	0.681	0.128
electrostatic	0.572	0.255	0.620	0.225	0.319	0.294
hydrophobic		0.176		0.188		0.165
donor		0.327		0.340		0.288
acceptor		0.131		0.143		0.125

[a] pIC_{50}, the negative logarithm of the molar IC_{50} concentration for cell growth inhibition; q^2, the cross-validated correlation coefficient; N, the optimal number of components; S. E. P., standard error of prediction; r^2, the non-cross-validated correlation coefficient; S. E. E., standard error of estimate; F, F-test value.

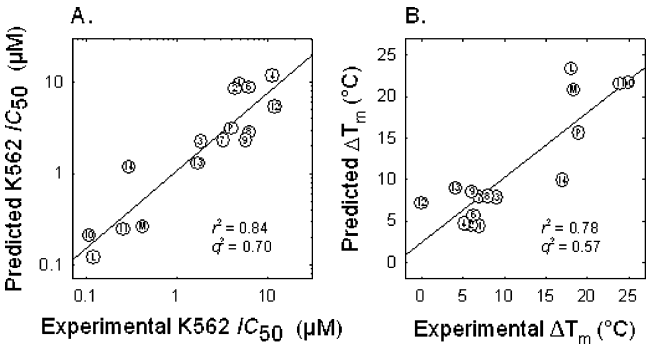

Figure 6. CoMSIA predictions for the effect of the anthrapyrazoles and mitoxantrone on IC_{50} for growth inhibition of K562 cells (A) and the increase in the DNA melt temperature ΔT_m (B). The straight lines are the regression lines for the predictions. The anthrapyrazoles are identified by the numbers inside the symbols, and losoxantrone, piroxantrone, and mitoxantrone are identified as L, P, and M, respectively.

alignment used were good predictors of the activity. The CoMFA and CoMSIA q^2 values of 0.593 and 0.570, respectively, for the ΔT_m data were, however, smaller than those for the biological data. CoMFA and CoMSIA were also carried out on the topoisomerase IIα IC_{50} data, and much lower q^2 values of 0.305 and 0.147, respectively, were found (Table 2). This result was consistent with the lack of correlation between the K562 IC_{50} and topoisomerase IIα IC_{50} data shown in Figure 2B. CoMFA and CoMSIA of the K562 IC_{50} data carried out on aligned structures in the lowest-energy conformations obtained with the SYBYL CONFORT module yielded lower q^2 values (0.530 and 0.401, respectively) than the q^2 values from the alignments obtained from the docking of the anthrapyrazoles into DNA. This result can be interpreted to mean that the conformations obtained from the docking into DNA are closer to the biologically active conformations.

For the K562 IC_{50} data, the electrostatic contribution to the CoMFA field was 57.2% compared to 42.8% for the steric contribution (Table 2). The ΔT_m data had a similar distribution. The CoMSIA, in addition to the steric and

electrostatic contributions to the field, measures hydrophobic and hydrogen-bond donor and acceptor contributions to the field. For both the K562 IC_{50} data and the ΔT_m data, hydrogen-bond donor contributions to the CoMSIA-calculated fields make the largest contribution, while electrostatic contributions were in both cases a close second. The isocontour diagrams of the hydrogen-bond donor and electrostatic field contributions to the K562 IC_{50} data ("stdev*coeff") were mapped onto the most potent anthrapyrazole AP-10 in Figure 4C and D, respectively. The green contours indicate regions that increase activity, and the red contours indicate regions that decrease activity. In the case of the hydrogen-bond donor field (Figure 4C), the green contour was localized close to the nitrogens of the two side chains, which suggests that protons on these side chains act as hydrogen-atom donors and contribute positively to the activity of the anthrapyrazoles. The results of the docking of AP-10 into DNA (Figure 4A) were in good agreement with this CoMSIA result, as docking resulted in two hydrogen bonds being formed from the secondary and tertiary nitrogens of the two side chains of AP-10 to the oxygen and a nitrogen atom of the guanine base. The smallest CoMSIA field contributions for both the K562 IC_{50} data and the ΔT_m data were the steric terms at 11.1% and 10.3%, respectively. This result probably reflects the fact that the anthrapyrazoles are planar molecules that easily intercalate into DNA without much steric hindrance. Modeling (Figure 4A) also showed that the side chains fit easily into either the major or the minor grooves of DNA without steric hindrance. The CoMSIA electrostatic plots shown in Figure 4D contain two areas of green contours located close to the protonated nitrogen atoms of the two amino side chains, indicating that the protonation of the amino side chains was important for the activity of the anthrapyrazoles.

4. DISCUSSION

The results of this study of a series of anthrapyrazole compounds showed that they potently inhibited the growth of K562 cells. The parent compounds of this group, losoxantrone and piroxantrone, which have both been tried in clinical trials[1−3,41−43] likely exert their cell growth inhibitory effects by acting as DNA topoisomerase II poisons.[7,8] The fact that cell growth inhibition was not correlated with inhibition of topoisomerase IIα-mediated catalytic decatenation activity suggests that the catalytic inhibition of topoisomerase II was not the primary mechanism by which these compounds act. This result does not rule out that the anthrapyrazoles were acting as topoisomerase II poisons. Intercalating compounds typically inhibit the catalytic activity of topoisomerase II, presumably by interfering with the formation of the DNA−topoisomerase II complex.[36] Because we did show that most of the anthrapyrazoles that could be evaluated were able to induce the formation of linear DNA through stabilization of a covalent topoisomerase IIα−DNA cleavable complex in a DNA cleavage assay, this result suggested that most of the new anthrapyrazoles also acted as topoisomerase II poisons similar to losoxantrone and piroxantrone.[7,8] This result was also supported by the general cross resistance (Table 1) that the anthrapyrazoles showed with the K/VP.5 cell line with a decreased level of topoisomerase IIα[14−17] as cells with less topoisomerase II in the cell produce fewer DNA strand breaks and topoisomerase II poisons are less lethal to these cells.[15,36] The fact that a high level of cross resistance was not seen may be due to the fact that the anthrapyrazoles also target other DNA processing enzymes because of their ability to intercalate into DNA.

The good correlation of K562 cell IC_{50} values with the ΔT_m values indicates that their inhibitory activity was due, in part, to their ability to bind to DNA. Using an X-ray structure of a doxorubicin−DNA complex (1DA9),[27] we showed that the structurally similar anthrapyrazoles could be docked into the doxorubicin binding pocket on DNA (Figure 4A). The affinity of the anthrapyrazoles for DNA as measured by ΔT_m was positively correlated (Figure 5C) with the DNA−ligand van der Waals external energy term from the GOLDScore fitness function, indicating that increased binding was associated with increased anthrapyrazole−DNA van der Waals interactions. Likewise, the potency of the anthrapyrazoles was also positively correlated with the external energy term (Figure 5A).

To further define the structural factors that result in high cell growth inhibitory potency for the anthrapyrazoles, 3D-QSAR CoMFA and CoMSIA were carried out in order to derive a model for the prediction of activity to aid in the synthesis of new, more active analogues. On the basis of a common substructure alignment (Figure 4B), both CoMFA and CoMSIA gave high-quality models based on their q^2 values (Table 2). The largest contributions to the CoMSIA field were hydrogen-bond donor and electrostatic contributions, in that order. The mapping of these fields onto the structure of AP-10, the most potent anthrapyrazole, showed that favorable contributions to the biological activity of these compounds was highly localized in the region around the protonated amino side chains. This conclusion is also supported by the docking results that showed that an amino side chain of AP-10 was able to act as hydrogen-bond donor to DNA (Figure 4A).

In summary, while the anthrapyrazoles were catalytic inhibitors of topoisomerase II, they likely exerted their cell growth inhibitory activity, at least in part, through their ability to act as topoisomerase II poisons. QSAR correlation and 3D-QSAR analyses showed the importance of anthrapyrazole−DNA van der Waals interactions, while 3D-QSAR CoMFA and CoMSIA showed that hydrogen-bond donor interactions and electrostatic interactions with the protonated amino side chains of the anthrapyrazoles led to high cell growth inhibitory activity.

ACKNOWLEDGMENT

Supported by grants from the Canadian Institutes of Health Research, the Canada Research Chairs Program, a Canada Research Chair in Drug Development to B.H., the Robert A. Welch Foundation (Grant AF-0005), the Herbert and Kate Dishman Endowment at Southwestern University to F.G., and a NIH grant (Grant CA90787) to J.Y.

REFERENCES AND NOTES

(1) Showalter, H. D.; Fry, D. W.; Leopold, W. R.; Lown, J. W.; Plambeck, J. A.; Reszka, K. Design, biochemical pharmacology, electrochemistry and tumour biology of antitumour anthrapyrazoles. *Anticancer Drug Des.* **1986**, *1*, 73−85.

(2) Judson, I. R. The anthrapyrazoles: A new class of compounds with clinical activity in breast cancer. *Semin. Oncol.* **1992**, *19*, 687−694.

(3) Gogas, H.; Mansi, J. L. New drugs. The anthrapyrazoles. *Cancer Treat. Rev.* **1996**, *21*, 541−552.
(4) Hartley, J. A.; Reszka, K.; Zuo, E. T.; Wilson, W. D.; Morgan, A. R.; Lown, J. W. Characteristics of the interaction of anthrapyrazole anticancer agents with deoxyribonucleic acids: Structural requirements for DNA binding, intercalation, and photosensitization. *Mol. Pharmacol.* **1988**, *33*, 265−271.
(5) Showalter, H. D.; Johnson, J. L.; Hoftiezer, J. M.; Turner, W. R.; Werbel, L. M.; Leopold, W. R.; Shillis, J. L.; Jackson, R. C.; Elslager, E. F. Anthrapyrazole anticancer agents. Synthesis and structure−activity relationships against murine leukemias. *J. Med. Chem.* **1987**, *30*, 121−131.
(6) Fry, D. W.; Boritzki, T. J.; Besserer, J. A.; Jackson, R. C. In vitro DNA strand scission and inhibition of nucleic acid synthesis in L1210 leukemia cells by a new class of DNA complexers, the anthra[1,9-cd]pyrazol-6(2H)-ones (anthrapyrazoles). *Biochem. Pharmacol.* **1985**, *34*, 3499−3508.
(7) Leteurtre, F.; Kohlhagen, G.; Paul, K. D.; Pommier, Y. Topoisomerase II inhibition and cytotoxicity of the anthrapyrazoles DuP 937 and DuP 941 (losoxantrone) in the National Cancer Institute preclinical antitumor drug discovery screen. *J. Natl. Cancer Inst.* **1994**, *86*, 1239−1244.
(8) Capranico, G.; Palumbo, M.; Tinelli, S.; Mabilia, M.; Pozzan, A.; Zunino, F. Conformational drug determinants of the sequence specificity of drug-stimulated topoisomerase II DNA cleavage. *J. Mol. Biol.* **1994**, *28*, 1218−1230.
(9) Herman, E. H.; Zhang, J.; Hasinoff, B. B.; Tran, K. T.; Chadwick, D. P.; Clark, J. R. J.; Ferrans, V. J. Comparison of the chronic toxicity of piroxantrone, losoxantrone and doxorubicin in spontaneously hypertensive rats. *Toxicology* **1998**, *128*, 35−52.
(10) Sissi, C.; Palumbo, M. Antitumor potential of aza-bioisosterism in anthracenedione-based drugs. *Curr. Top. Med. Chem.* **2004**, *4*, 219−230.
(11) Sissi, C.; Leo, E.; Moro, S.; Capranico, G.; Mancia, A.; Menta, E.; Krapcho, A. P.; Palumbo, M. Antitumor AZA-anthrapyrazoles: Biophysical and biochemical studies on 8- and 9-aza regioisomers. *Biochem. Pharmacol.* **2004**, *67*, 631−642.
(12) Showalter, H. D. H.; Johnson, J. L.; Hoftiezer, J. M. Heteroannulated-9,10-anthracenediones. The synthesis of substituted 5- and 7-chloroanthra[1,9-cd]pyrazol-6(2H)-ones, precursors to anticancer anthrapyrazoles. *J. Heterocycl. Chem.* **1986**, *23*, 1491−1501.
(13) Showalter, H. D. H.; Johnson, J. L.; Hoftiezer, J. M. The Synthesis of substituted 5- and 7-chloroanthra[1,9-*cd*]pyrazol-6(2*H*)-ones, precursors to anticancer anthrapyrazoles. *J. Heterocycl. Chem.* **1986**, *23*, 1491−1501.
(14) Ritke, M. K.; Yalowich, J. C. Altered gene expression in human leukemia K562 cells selected for resistance to etoposide. *Biochem. Pharmacol.* **1993**, *46*, 2007−2020.
(15) Ritke, M. K.; Allan, W. P.; Fattman, C.; Gunduz, N. N.; Yalowich, J. C. Reduced phosphorylation of topoisomerase II in etoposide-resistant human leukemia K562 cells. *Mol. Pharmacol.* **1994**, *46*, 58−66.
(16) Ritke, M. K.; Roberts, D.; Allan, W. P.; Raymond, J.; Bergoltz, V. V.; Yalowich, J. C. Altered stability of etoposide-induced topoisomerase II-DNA complexes in resistant human leukemia K562 cells. *Br. J. Cancer* **1994**, *69*, 687−697.
(17) Fattman, C.; Allan, W. P.; Hasinoff, B. B.; Yalowich, J. C. Collateral sensitivity to the bisdioxopiperazine dexrazoxane (ICRF-187) in etoposide (VP-16) resistant human leukemia K562 cells. *Biochem. Pharmacol.* **1996**, *52*, 635−642.
(18) Hasinoff, B. B.; Kozlowska, H.; Creighton, A. M.; Allan, W. P.; Thampatty, P.; Yalowich, J. C. Mitindomide is a catalytic inhibitor of DNA topoisomerase II that acts at the bisdioxopiperazine binding site. *Mol. Pharmacol.* **1997**, *52*, 839−845.
(19) Hasinoff, B. B.; Abram, M. E.; Barnabé, N.; Khelifa, T.; Allan, W. P.; Yalowich, J. C. The catalytic DNA topoisomerase II inhibitor dexrazoxane (ICRF-187) induces differentiation and apoptosis in human leukemia K562 cells. *Mol. Pharmacol.* **2001**, *59*, 453−461.
(20) Hasinoff, B. B.; Wu, X.; Yang, Y. Synthesis and characterization of the biological activity of the cisplatin analogs, *cis*-$PtCl_2$(dexrazoxane) and *cis*-$PtCl_2$(levrazoxane), of the topoisomerase II inhibitors dexrazoxane (ICRF-187) and levrazoxane (ICRF-186). *J. Inorg. Biochem.* **2004**, *98*, 616−624.
(21) Barnabé, N.; Hasinoff, B. B. High-throughput fluorescence flow injection topoisomerase II inhibition assay. *J. Chromatogr., B* **2001**, *760*, 263−269.
(22) Hasinoff, B. B.; Wu, X.; Krokhin, O. V.; Ens, W.; Standing, K. G.; Nitiss, J. L.; Sivaram, T.; Giorgianni, A.; Yang, S.; Jiang, Y.; Yalowich, J. C. Biochemical and proteomics approaches to characterize topoisomerase IIα cysteines and DNA as targets responsible for cisplatin-induced inhibition of topoisomerase IIα. *Mol. Pharmacol.* **2005**, *67*, 937−947.
(23) Burden, D. A.; Froelich-Ammon, S. J.; Osheroff, N. Topoisomerase II-mediated cleavage of plasmid DNA. *Methods Mol. Biol.* **2001**, *95*, 283−289.
(24) Priebe, W.; Fokt, I.; Przewloka, T.; Chaires, J. B.; Portugal, J.; Trent, J. O. Exploiting anthracycline scaffold for designing DNA-targeting agents. *Methods Enzymol.* **2001**, *340*, 529−555.
(25) McGhee, J. D. Theoretical calculations of the helix-coil transition of DNA in the presence of large, cooperatively binding ligands. *Biopolymers* **1976**, *15*, 1345−1375.
(26) *SYBYL 7.0*; Tripos Inc.: St. Louis, MO.
(27) Leonard, G. A.; Hambley, T. W.; McAuley-Hecht, K.; Brown, T.; Hunter, W. N. Anthracycline−DNA interactions at unfavourable base-pair triplet-binding sites: Structures of d(CGGCCG)/daunomycin and d(TGGCCA)/adriamycin complexes. *Acta Crystallogr., Sect. D* **1993**, *49*, 458−467.
(28) *GOLD 3.1*; CCDC Software Ltd.: Cambridge, U. K.
(29) Verdonk, M. L.; Cole, J. C.; Hartshorn, M. J.; Murray, C. W.; Taylor, R. D. Improved protein−ligand docking using GOLD. *Proteins* **2003**, *52*, 609−623.
(30) Berman, H. M.; Westbrook, J.; Feng, Z.; Gilliland, G.; Bhat, T. N.; Weissig, H.; Shindyalov, I. N.; Bourne, P. E. The Protein Data Bank. *Nucleic Acids Res.* **2000**, *28*, 235−242.
(31) Clark, M.; Cramer, R. D., III; Van Opdenbosch, N. Validation of the general purpose Tripos 5.2 force field. *J. Comput. Chem.* **2004**, *10*, 982−1012.
(32) Wang, J.; Cieplak, P.; Kollman, P. A. How well does a restrained electrostatic potential (RESP) model perform in calculating conformational energies of organic and biological molecules? *J. Comput. Chem.* **2000**, *21*, 1049−1074.
(33) Cramer, R. D., III; Patterson, D. E.; Bunce, J. D. Comparative molecular field analysis (CoMFA). 1. Effect of shape on binding of steroids to carrier proteins. *J. Am. Chem. Soc.* **1988**, *110*, 5959−5967.
(34) Kubinyi, H.; Folkers, G.; Martin, Y. C. *3D QSAR in Drug Design*; Kluwer Academic: Dordrecht, The Netherlands, 1998.
(35) Klebe, G.; Abraham, U.; Mietzner, T. Molecular similarity indices in a comparative analysis (CoMSIA) of drug molecules to correlate and predict their biological activity. *J. Med. Chem.* **1994**, *37*, 4130−4146.
(36) Fortune, J. M.; Osheroff, N. Topoisomerase II as a target for anticancer drugs: When enzymes stop being nice. *Prog. Nucleic Acid Res. Mol. Biol.* **2000**, *64*, 221−253.
(37) Li, T. K.; Liu, L. F. Tumor cell death induced by topoisomerase-targeting drugs. *Annu. Rev. Pharmacol. Toxicol.* **2001**, *41*, 53−77.
(38) Hasinoff, B. B.; Wu, X.; Begleiter, A.; Guziec, L.; Guziec, F.; Giorgianni, A.; Yang, S.; Jiang, Y.; Yalowich, J. C. Structure−activity study of the interaction of bioreductive benzoquinone alkylating agents with DNA topoisomerase II. *Cancer Chemother. Pharmacol.* **2006**, *57*, 221−233.
(39) Tewey, K. M.; Rowe, T. C.; Yang, L.; Halligan, B. D.; Liu, L. F. Adriamycin-induced DNA damage mediated by mammalian DNA topoisomerase II. *Science* **1984**, *226*, 466−468.
(40) Perola, E.; Charifson, P. S. Conformational analysis of drug-like molecules bound to proteins: An extensive study of ligand reorganization upon binding. *J. Med. Chem.* **2004**, *47*, 2499−2510.
(41) Diab, S. G.; Joshi, A.; Cobb, P. W.; Eckhardt, S. G.; Rodriguez, G. I.; Kraynak, M.; Finizio, M.; Rowinsky, E. K. A phase I and pharmacokinetic study of losoxantrone and paclitaxel in patients with advanced solid tumors. *Clin. Cancer Res.* **1999**, *5*, 299−308.
(42) Talbot, D. C.; Smith, I. E.; Mansi, J. L.; Judson, I.; Calvert, A. H.; Ashley, S. E. Anthrapyrazole CI941: A highly active new agent in the treatment of advanced breast cancer. *J. Clin. Oncol.* **1991**, *9*, 2141−2147.
(43) Ingle, J. N.; Kuross, S. A.; Mailliard, J. A.; Loprinzi, C. L.; Jung, S.-H.; Nelimark, R. A.; Krook, J. E.; Long, H. J. Evaluation of piroxantrone in women with metastatic breast cancer and failure on nonanthracycline chemotherapy. *Cancer* **1994**, *74*, 1733−1738.

CI060056Y